Antecedent rainfall as a critical factor for the triggering of debris flows in arid regions

Shalev Siman-Tov[1], Francesco Marra[2,3]

[1]Geological Hazards Division, Geological Survey of Israel, Jerusalem, 9692100, Israel
5 [2]Department of Geosciences, University of Padova, Italy
[2]Institute [3]Institute of Atmospheric Sciences and Climate, National Research Council, Bologna, Italy

Correspondence to: Shalev Siman-Tov (shalevst@gsi.gov.il)

Abstract. In arid regions, debris flows (DFs) are occasionally observed when heavy rainfall hits steep slopes with unconsolidated materials. Despite the related hazards, not much is yet known about the critical rainfall conditions for DF
10 initiation in dryland areas, mainly due to lack of observations and data. In this study, we use high-resolution digital surface models and orthophotos to detect DFs on the arid slopes of the Dead Sea north-western margins, and weather radar rainfall estimates for the characterization of the triggering and non-triggering storms. We identify deposits from over 40, relatively small, DFs that occurred between 2013 and 2019. We divide them into four groups based on their spatial distribution and triggering period, and identify the most likely initiating triggering storms based on weather radar data and additional
15 information and social media information. We show that the DFs were likely triggered by an intense convective cell (lasting less than <45 min) which was preceded by non-negligible rainfall amounts (~(about 10 mm) delivered during the storm. Comparing triggering and non-triggering storms, we observed that rain intensity alone is insufficient to explain the phenomena, and discuss the possibility that antecedent rainfall could represent a critical factor for the triggering of DFs in steep slopes of arid environments.

20 **1 Introduction**

Debris flows (DF) are gravity driven, downslope flows of water and sediment mixtures (Takahashi, 2014; Iverson, 1997). They constitute one of the most impactful natural hazards in mountainous regions, with casualties and damage to infrastructures. Debris flows commonly follow pre-existing channels and often end at lower gradients, where lobes of sediments are deposited at the mountain front. Cohesionless sediments that cover steep mountain slopes (e.g., colluvium or pyroclastic deposits) usually
25 provide the debris material. The typical morphological characteristics of DF include levees along the channel sides, terminal lobes, coarse and poorly sorted grains, and U-shape flow channel with a low depth/width ratio (Costa, 1988; Pierson, 2005; Wells and Harvey, 1987). Debris flows are typically triggered by heavy precipitation or, more rarely, by sudden snow or ice melt in mountainous and volcanic areas. Short-duration convective storms constitute a key factor in DF triggering because

high rain intensities may easily exceed the soil infiltration capacity causing surface runoff, leading to the triggering (Church
30   and Miles, 1987; Iverson, 2000; Mostbauer et al., 2018; Dunkerley, 2021; Caine, 1980).

Debris flows can occur in arid and semiarid regions (Webb et al., 1989; Blackwelder, 1928; Stolle et al., 2015; Coe et al., 1997; Moreiras and Sepúlveda, 2022; Sepúlveda et al., ~~2014~~2006, ~~2006~~2014) as a result of the heavy rainfall extremes characterizing these areas (Marra and Morin, 2015) and of the quick runoff response typical of arid and unvegetated soils (Zoccatelli et al., 2019). In the arid northern Chile, Sepulveda et al. (2006) identified possible relations between large-scale
35   climatic drivers, such as El Nino episodes, and debris flow triggering. Similarly, Sepulveda et al. (2014) closely examined a debris flow triggering by an extreme rainstorm in the same region. ~~For example~~In addition, DFs were extensively studied in the semiarid to arid regions of the Grand Canyon slopes in northern Arizona, where they mostly occur when runoff triggers failures in colluvium during intense rainfall (Griffiths, 2004; Melis et al., 1995; Webb et al., 1989). Based on the available data, sustained intensity exceeding 20 mm h^{-1} and a total rainfall of 25 to 50 mm can be considered as the minimal threshold
40   for DF triggering in this area (Melis et al., 1995; Webb et al., 1989; Melis and Webb, 1993).

This study is conducted along the steep arid slopes of the Eastern Judean desert, on the western margins of the Dead Sea. ~~Albeit rare,~~ DF activity in this region can be particularly dangerous to human settlements, main roads and nature reserve infrastructures. In addition to their destructive potential, DFs have here a major influence on slope morphology and alluvial fan build up (Ben David-Novak et al., 2004; Ben David-Novak, 1998; Ahlborn et al., 2018; Enzel, 2001). Ahlborn et al. (2018),
45   in particular, examined graded layer_s deposited during the Holocene associated to DFs, and observed periods with drier conditions and increased DF activity and periods with wetter conditions and lower DF activity. They associated this counter intuitive observation to changes in the synoptic conditions of the Eastern Mediterranean, raising the question whether the future occurrence of DF, and therefore of the related hazards, could be affected by the ongoing climate change. While most of the critical environmental conditions for DF triggering are met, e.g., unconsolidated sediments on steep slopes, it seems that
50   the most limiting factor in this area is precipitation (Ben David-Novak et al. 2004). The only studies about modern DFs in the area focused on a few rainstorms occurred between the years 1987-1997 (Ben David-Novak, 1998; Ben David-Novak et al., 2004). They suggest that minimum conditions for DF triggering consist of rainfall intensity exceeding 30 mm h^{-1} for duration of at least one hour, although the typical lifetime of convective cells in the area is shorter (around 20-40 min according to Belachsen et al. (2017)). Moreover, the characteristics of the rainfall occurred before the triggering cells were not considered
55   in previous studies (e.g., Ben David-Novak et al., 2004).

The possible importance of antecedent ~~precipitation~~ rainfall on landslide triggering was extensively studied for non-arid environments (e.g. Glade et al. 2000; Aleotti 2004; Guzzetti et al. 2008; Frattini et al. 2009; Kim et al. 2021). It was suggested that ~~I~~in tropical areas ~~(Brand, 1992) and~~where slopes are covered by permeable soils or sediments,~~grains having large inter-particle void space (Corominas and Moya, 1999; Brand, 1992), it was suggested that~~ antecedent rainfall is less important ~~than~~
60   ~~in other environments, possibly because of the high permeability of the local soils that~~ in reduc~~ing~~es the potential of failure

(Rahardjo et al., 2001; Brand, 1992; Corominas and Moya, 1999). ~~Conversely, t~~To the best of our knowledge, however, the effect of antecedent rainfall on DF triggering in arid regions was not yet explored, probably due to the lack of DF observations and of adequate rainfall data. An improved knowledge of the rainfall characteristics leading to DFs in arid regions is critical for the understanding of the triggering mechanisms and for improving our ability to provide effective early warnings. In this paper we aim at improving our understanding of the critical conditions for DF triggering in arid areas by combining high-resolution topography models, field surveys, and an advanced archive of high-resolution gauge-adjusted radar rainfall estimates which comprises both triggering and non-triggering events.

The paper is organized as follows. After introducing the reader to the study area (Section 2), we present our mapping of DFs in the study area (Section 3) and the identification of the most likely triggering rainfall (Section 4). We close by discussing the role of antecedent rainfall for DF triggering and the potential implications for DF frequency in the region (Section 5). We close with a collection of the main conclusions (Section 6).

2 Study Area

The study area is located on the east side of the northern Judean desert, on the north-western escarpment of the Dead Sea basin (Fig. 1). We focus on the portion of the escarpment limited to the north by the Og Wadi and to the south by the Hever Wadi (Fig. 1). The slopes are mostly composed of carbonate rock layers including hard limestone and dolomites, interbedded with weak marl layers. These exposed carbonate rocks of the Judean Group units deposited on the regional carbonate platform during the Cretaceous (Sneh et al., 2000; Raz, 1983; Mor, 1987; Roth, 1969). The slope angle is usually gentle (5°-30°) at the bottom and becoming steep ~~(>~~(above 30°) or vertical at its upper parts (Fig. 2). This escarpment is a result of normal faulting followed by ongoing erosional processes along the margins of the Dead Sea basin since the late Miocene to early Pliocene (Garfunkel and Ben-Avraham, 1996; Garfunkel et al., 1981; Haviv et al., 2006).

The ~40 km long studied escarpment can be generally divided into three parts: lower soft sediments, middle colluvium and upper cliffs (Fig. 2). In many places along the lower parts of the escarpment (altitude over 300 m below the mean sea level), the carbonate rock slopes are covered by lacustrine and fluvial sediments (Fig. 2c), deposited during high lake stands in the Pliocene-Pleistocene periods (Bartov et al., 2002, 2007; Sneh, 1979; Begin et al., 1980). Many of these exposures are soft and/or cohesionless, mostly composed of carbonate pebbles. The upper third of the escarpment, usually the steepest, is rocky and composed of hard carbonate rocks (mostly dolomites). The middle part of the escarpment is mostly covered by colluvium composed of fragments originated from the rock mass above (Fig. 2b). While the colluvium coverage may change from place to place along the escarpment, it is still abundant and does not represent a limiting factor for DF triggering in the study area. The colluvium thickness is changing laterally with an observed maximum value of a few meters. At the surface, the colluvial material is usually grain supported with increasing amounts of fine particles at depth of a few tens of centimetres. The colluvium fine fraction ~~(<~~(less than 2 mm) is dominated by crashed dolomites and some quartz, calcite and phyllosilicates

probably from eolian source. This fine material becomes muddy and unstable once exposed to water. The lacustrine and fluvial sediments together with the colluvial deposits constitute the typical source material of DFs in the study area (Ben David-Novak et al., 2004).

95 In the study area, the average annual precipitation ranges between 50 to 100 mm, based on constantly recording rain gauges for the years 1991-2020 (https://ims.gov.il/en/ClimateAtlas; see Fig. 1 for station locations). This variation in precipitation has a clear geographic gradient, with lower amounts observed in the southern part, caused by the decreasing frequency of precipitation, and in the eastern part, caused by the orographic shading of the Judean mountains. The rainy season is between October to May, with more frequent rainstorms during the winter (December to February), generally related to Mediterranean
100 cyclones. Some less frequent, but more intense rainstorms occur during the autumn and spring months, generally related to Active Red Sea Troughs (ARST). While Mediterranean cyclones are characterized by regional scale rainfall that decreases southward and eastward in the study area, ARSTs produce heavy and localized convective rain cells which tend to occur more uniformly across our domain (Armon et al., 2019; Hochman et al., 2022). On rare occasions, systems of tropical origin, termed Tropical Plumes, may hit the region with large amounts of precipitation at the regional scale (Tubi and Dayan, 2014).

105
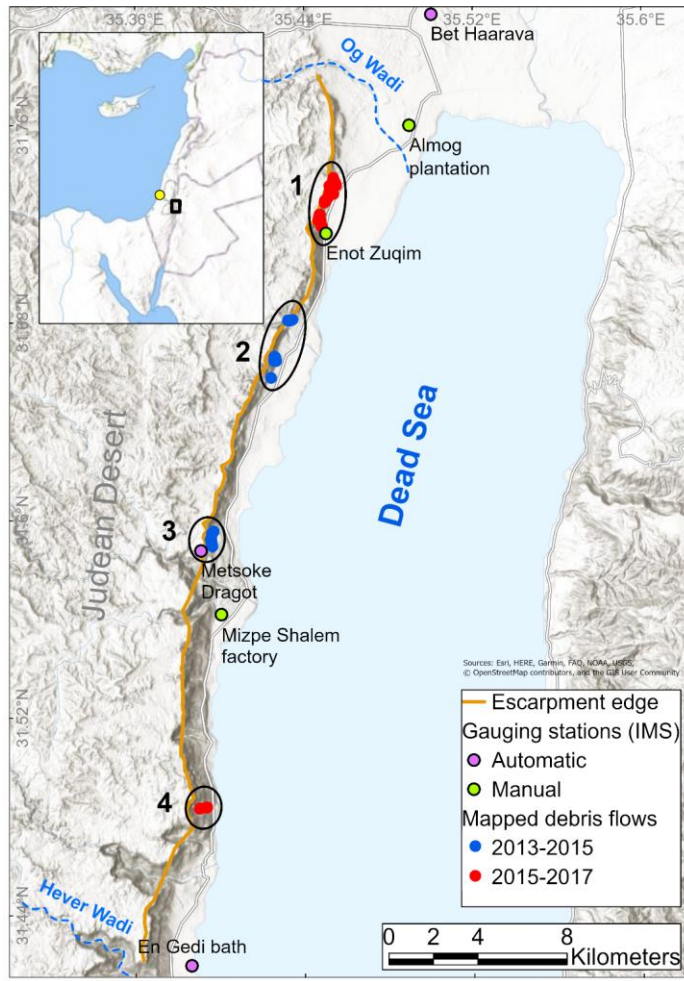
Figure 1: Map of the study area. An inset shows the location of the study area (black rectangle) and of the weather radar (yellow point) on the eastern Mediterranean map. The 43 DF deposits were mapped using elevation-difference maps from the years 2013-2015 (in blue) and 2015-2017 (in red). The deposits were classified into four groups (black ellipse). Rain gauge stations of the Israel meteorological service are marked in purple and green points for automatic (10-min) and manual (daily) stations, respectively.
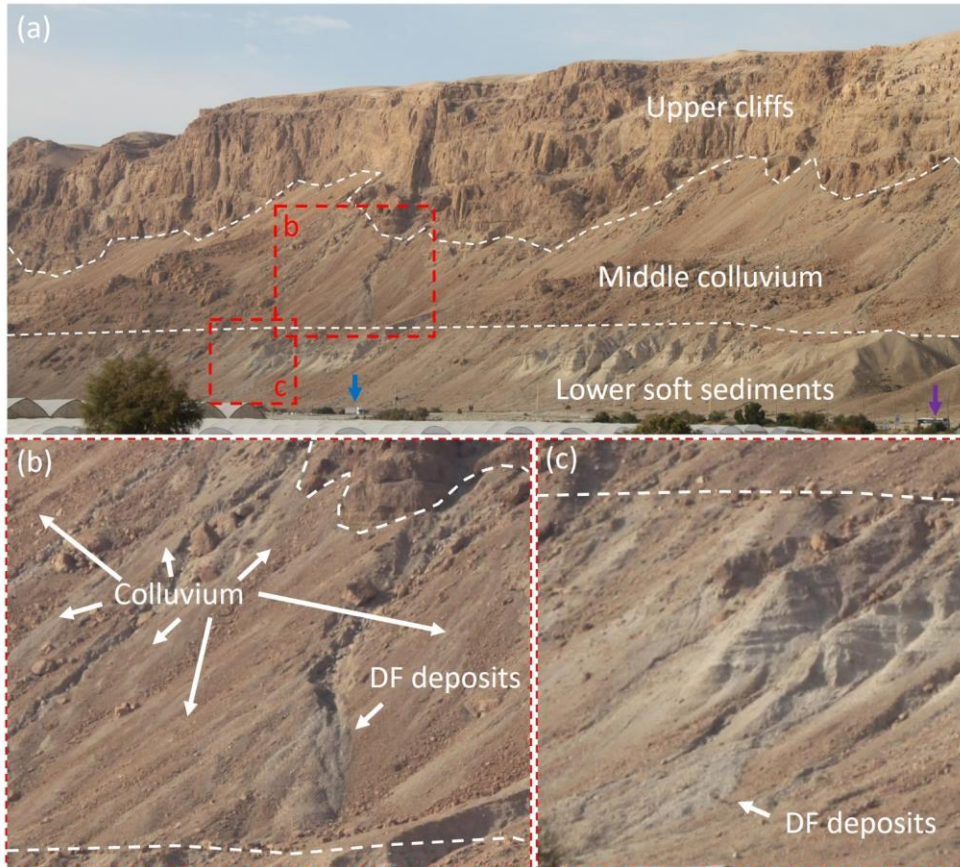
Figure 2. The studied escarpment and the observed DF deposits. (a) The northern part of the study area where group 1 DFs were observed. The escarpment is generally divided into three parts: the upper cliffs, middle colluvium, and lower soft sediments. A truck and a bus are marked for scale by blue and purple arrows, respectively. The extent of the zooming-in photos are marked by red rectangles. (b) A section of the middle colluvium part of the escarpment. Colluvium cover (some are pointed by white arrows) with some large boulders is cut by small ephemeral streams that ends with DF deposits. The source material is usually clearly seen in the colluvium above these deposits. (c) A DF lobe at the end of a short ephemeral stream. The deposits source from the light-color lacustrine sediments.

3 Debris flows detection and characterization

120 **3.1 Mapping methods**

Aiming to detect modern, natural changes resulting from mass-wasting processes along the studied escarpment, we compared aerial photos and high-resolution digital surface models ~~(DSM)~~ that were available for the years 2013-2019. During that period, no additional instrumentation was installed in the study area to identify triggered DFs. We therefore used the available orthophotos and digital surface models~~DSMs~~ to map new DF deposits and to minimize the time interval of triggering. The

125 digital surface models~~DSMs~~ are the product of airborne light detection and ranging (LiDAR) scans, having spatial resolution of 0.5 m pixel^{-1} with spatial uncertainty ~~<~~lower than 1 m. In the vertical dimension, the digital surface models~~DSMs~~ absolute elevation error is ~~<~~lower than 0.35 m. We obtained digital surface models~~DSMs~~ of every second year: 2013 (scan date May 29-31, 2013), 2015 (Apr-May 2015), 2017 (May 12, 2017), 2019 (Sep 29-30, 2019). In order to identify topography changes, we subtract the earlier digital surface model~~DSM~~ from the more recent one. The new raster of elevation-differences, also

130 known as ~~DEM (~~digital elevation model~~)~~ of Difference (DoD), should have positive values if material added, negative for deficiency, and around zero for no change (Williams, 2012; Morino et al., 2019). In general, this is the case apart from two exceptions: 1) the average difference value for stationary areas is non-zero, suggesting a vertical offset of a few tens of centimeters; 2) noisy results around high relief lines (cliffs). The first issue, probably caused by a systematic error of the digital surface model~~DSM~~ elevation, is expected to have a minor influence on our results: to ensure a better detection we computed

135 the mean offset by averaging several stationary areas and subtract it from the DoD. The second issue mostly affects the cliff area, and the cliff lineaments in particular, and consists of noisy raster values (neighbouring cells with values above and below zero). This artifact is not expected to affect our detection, because DFs are recognized by nearby regions with similar values, so that noisy areas can be easily excluded. However, some tiny DF deposits are possibly missed by this procedure, especially those with area smaller ~~then~~ than ~25 m^2 and average thickness smaller than ~~~~~0.6 m.

140 In order to narrow our uncertainty in the estimated time of triggering (otherwise only limited by the time interval between airborne LiDAR scans), we used orthophotos, media and social network documentation. In terms of aerial photos, we mostly use geometrically corrected (orthophotos) with resolution of 0.25 m pixel^{-1}, from the years 2015 (photos taken in Jun-Jul 2015) and 2016 (photos taken Apr 15-30, 2016). Nevertheless, for most cases, the exact timing of the DF triggering was unknown and we had to identify the most probable triggering date as described below.

145 **3.2 Identified debris flows and field observations**

We identified 43 DF deposits that occurred between the years 2013-2019. Two additional deposits were classified as rockfalls and removed from the analyses. The DF deposits are located along small ephemeral streams that drain the cliff area above

them and present evidence of previous DF activity. This suggests that they were mobilized by flow events and therefore considered as DFs, as suggested by Hungr et al. (2001). The DFs we examine are small-sized, with a maximum runout distance (between the source location and deposit) of a few tens of meters. The areal extent of each DF deposit ranges between 10 and 1000 m^2 with an average value of 150 m^2 and elongated shapes of ~about 30 m in length and ~5 m in width. Although during the studied period (2013-2019), only small-size and short runout distance DFs could be clearly mapped, longer runout distance DFs from past events are observed along the studied escarpment (Fig. 3). In principle, it is possible that larger DFs did occur during the studied period (2013-2019), but subsequent road construction and floods blurred the DF tracks. This made it impossible for us to detect them by means of DoDs and to verify the nature of the phenomena (e.g., distinguishing between DF and flash floods) based on field surveys. This is to emphasize that, although the studied DFs are relatively small, their triggering mechanism is similar to potentially more hazardous DFs. All the mapped DFs in this study are of the first to second stream order, following the "top down" system division. Their drainage basins are extremely small, usually limited to the cliff itself or to a kilometer west of the clifftop at most. The spatial extent of each DF deposit was mapped into a polygon based on the DoDs (positive values for added material). These polygons were primarily grouped according to the time interval they were triggered (two years intervals based on the LiDAR scans): 17 DFs between 2013 and 2015, 26 DFs between 2015 and 2017, while no deposits were identified for the period 2017-2019 (Fig. 1).

Aiming to verify that the mapped deposits are indeed the result of DFs, we explored their structure and morphology in the field (Fig. 4). In many cases, the DFs are located on very steep slopes (20°-40°) with limited access. All mapped deposits and their related upstream erosional scours (i.e., depressions along the streams where the missing material is the source for the debris material) are located along or at the edge of short ephemeral streams that drain the cliff. The deposited sediments are poorly sorted, a principal characteristic that distinguished DFs from water-laid sediments. Distal lobes, also known as depositional lobes, are observed for all the mapped deposits at the toe of the flow. For some cases, also side lobes are observed upstream, along the flow path (Figs. 4e-4f). Levees, usually a few tens of centimeters high, are occasionally observed on both sides of the channel; although they are barely seen in the DoDs., ; iIn the field, the greyish levees are clearly distinguished from the surrounding brownish colluvium (Figs. 3 and 4d). These levees consist of relatively large fragments, similar to those found in the lobes. All these elements suggest that these deposits were caused by DFs.

For most of the mapped DFs (N=37 cases), the deposits consist of angular dolomite and limestone fragments, unsorted grains with a maximum size of a few tens of centimetres. This deposit composition reflects the colluvium composition above it, which mostly composed of the upper escarpment cliffs and some aeolian fine particles. Hence, the source for the debris material is the talus at the base of theses cliffs (Fig. 2b). Differently, in fewer cases DFs (N=6 cases) located at the bottom of the lower step on the escarpment, the deposits consisted of rounded fragments, apparently derived from the nearby cliff of lacustrine and conglomerate sediments (Fig. 2c). These same two sources of debris materials were also reported by a previous study in the region (Ben David-Novak et al., 2004).

180 We divided the mapped DFs into four groups based on the triggering time interval and on their spatial distribution across the study area, with the assumption that each group has been triggered by an individual convective cell (Fig. 1). While it is in theory possible that nearby DFs were triggered by different storms over a short period of time, we deem this possibility highly unlikely due to the rare occurrence of DFs in the region. Conversely, a specific storm, that may last for a few days, could represent the trigger of several groups. However, since the distances between groups observed in the same 2-year time intervals

185 is always greater than 8 km, and the typical scale of convective cells in the region is smaller (Belachsen et al., 2017; Marra and Morin, 2018), these groups were likely triggered by different convective cells. As we will see, this is possibly the case of our groups one and four, which occurred in the northern and southern parts of the study area, respectively (Fig. 1).

Figure 3. An example of debris flow deposits triggered prior to 2013. A distal lobe (white arrow), two levees (blue arrows) and a wide and shallow channel in-between them at the end of ephemeral stream drained the cliff area.
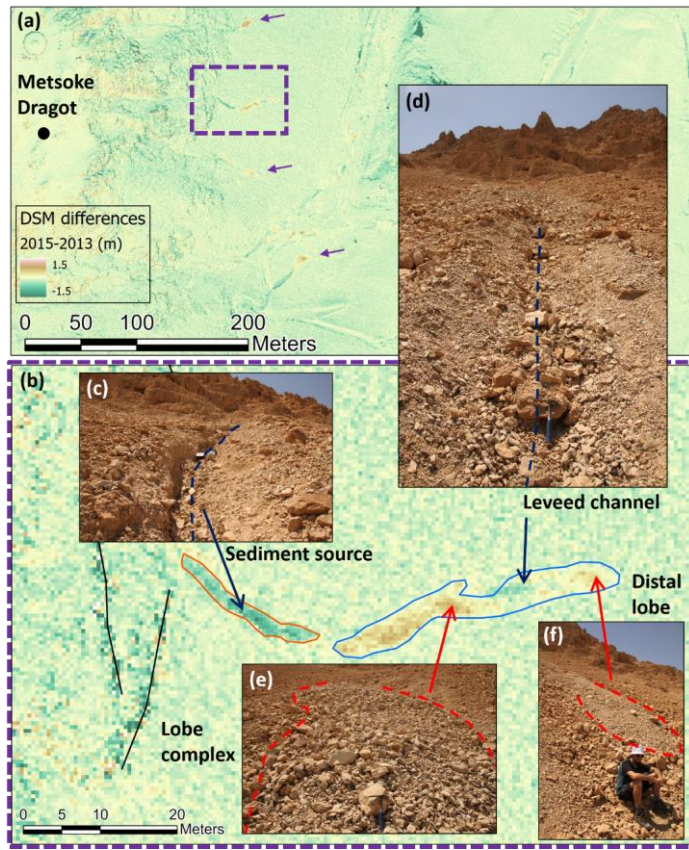
190 **Figure 4: Mapping and characterization of debris flows in the field and the topographic models.** (a) Natural changes in the steep slope east to Metsoke Dragot village as reflected from the DoD of the years 2013-2015. Brown shades suggest newly deposited materials while dark green shades represent new depressions. More details on the DF in the purple rectangle are shown in panels b to f. Arrows mark three additional DF deposits. (b) Zoom in to the DF area, where the source of the debris material and the elongated deposits are well seen in the map. Upper slope Cliffs (black lines) are noisier in the DoDdifference maps. (c) A channel (dashed line shows its path) incised in the
195 unconsolidated colluvium. (d) The DF channel with parallel levees on its margins. (e) Deposits of the lobe complex. (f) The distal lobe.

4 Rainfall leading to debris flows

We introduce here three concepts that we will use to characterise the properties of the ~~precipitation~~ rainfall that led to DF initiation (see Fig. 5). We define as "~~initiating~~ *triggering* storm" the storm event during which a DF is initiated. To this end, storms are defined as wet periods separated by at least 5 days of dry weather (i.e., 120 hours with less than 0.1 mm h⁻¹ in the radar data; note that given the climatology of the area with very few storms per year, there is little sensitivity to this choice). We define as "*triggering cell*" the high-intensity convective cell that likely provided the final trigger to the DF initiation. Last, we define as "*antecedent ~~precipitation~~rainfall*" the rainfall observed before the triggering cell and during the ~~initiating~~ triggering storm (i.e., between the beginning of the ~~initiating~~ triggering storm and the beginning of the triggering cell).
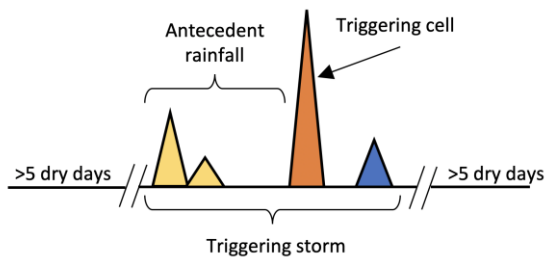
Figure 5: Schematic representation of the triggering storms showing: triggering storm, triggering cell, and antecedent rainfall. The colored triangles represent the rainfall throughout the triggering storm: antecedent rainfall (yellow), triggering cell (orange), and rainfall after the DF triggering in blue.

4.1 Rainfall data

Our mapping of natural changes along the steep escarpment between the years 2013-2019 suggests that the majority of mass wasting events were caused by DFs. We used both rainfall stations located within or in close proximity to the study area and the weather radar of the Israeli meteorological service (Fig. 1) to identify and characterize the triggering storms. We used the rainfall data from two types of stations (https://ims.gov.il/en/stations) as shown in Fig. 1: 1) Automatic rain gauges with a time resolution of ten minutes (from north to south: Bet Haarava, Metsoke Dragot, En Gedi bath); 2) daily rain gauges (from north to south: Almog plantation, Enot Zuqim, Mizpe Shalem factory). Weather radar data are used to assess the rainfall conditions above the DFs, and rain gauge data are used to constrain and validate the radar data on a regional scale.

The weather radar (https://ims.gov.il/en/node/193) gives rainfall intensity maps every five minutes at 500 m resolution, and allows spatial analysis of the event. In particular, weather radar data is essential to capture the DF triggering rainfall conditions especially in convective environments. In fact, ~~as~~ rain gauges tend to systematically underestimate ~~the rainfall corresponding to~~ the DF triggering rainfall ~~locations~~because they sample precipitation fields away from the triggering locations and because these fields are characterised by sharp spatial variability and necessarily have high intensities over the triggering locations

(Marra et al., 2016; Destro et al., 2017; Marra et al., 2014; Nikolopoulos et al., 2014, 2015). Weather radar data was provided by the Israel Meteorological Service and elaborated following the procedures described in Marra et al. (2022), which include physically-based corrections and empirical adjustments based on rain gauge climatology. In addition, in order to reduce the bias typically observed in our study area (e.g. see Marra et al., 2022), we gauge-adjusted the radar data of each storm (see definition above) using data from the daily rain gauges described above (e.g. see Rinat et al., 2021). Despite these careful adjustments, the radar samples the study area about 3 km above the ground (see Marra et al. 2022) so that rainfall at the ground could be misplaced by a few hundreds of meters in case of strong winds in the lower atmosphere. This may cause some errors in the estimation of rain intensities; in particular, because of the typical characteristics of DF-triggering convective rainfall (Marra et al., 2016), we expect that in these cases, our evaluation could be underestimated. While this does not affect our findings, some caution is to be used on the rain intensity values we report. It is worth noting that the previous studies in the region (e.g., Ben David-Novak et al., 2004) were based on data from a different weather radar, which was however located not far from the one used here; thus, the same caveats are to be used in interpreting those quantitative estimates.

4.2 Identification of the most likely ~~initiating~~ triggering storms

Since the study area was documented by airborne LiDAR roughly every second year, we search for all the potential ~~initiating~~ triggering storms that could have triggered the DFs during the time intervals between two subsequent scans (Fig. ~~5~~6). For the analysis, we consider the location of each DF at the center of its mapped deposit. The many streams that drain the cliff have a very small drainage area (maximum distance between the deposits and the basin head 750 m). As the weather radar resolution is 500x500 m^2, we can assume that the rainfall observed by the radar in correspondence to the deposit location represents a good approximation of the rainfall over the drainage basin (Marra et al., 2014).

Following this procedure, we plot for each DF, the five-minute rainfall intensity versus time, for its relevant two years interval (Fig. ~~5~~6). For example, for a DF from group number three, mapped east to Metsoke Dragot, we used the radar data for the years 2013-2015. Note that gaps in the radar data are possible because of technical issues, and because during dry periods the radar is often turned off. In order to make sure that we did not miss critical storms, we compared the radar data with rain gauge stations. During the period of 2013-2017, we found only two storms (Jan 8-9, 2016 and Jan 27-29, 2017) during which the radar was off.

We picked potential ~~initiating~~ triggering storms, by isolating those storms in which the peak rainfall intensities exceeded 10 mm h^{-1}, and the peak 30-minute intensity (average intensity over 30 minutes periods) exceeded 5 mm h^{-1} (Fig. ~~5~~6). Recalling that previous studies reported thresholds of 30 mm h^{-1} over 1-hour periods, and that 10 mm h^{-1} is often regarded as a threshold for defining convective precipitation (e.g., Peleg and Morin 2012), this selection is based on rather low intensities, i.e., it ensures we will select all the potential ~~initiating~~ triggering storms and it diminishes the possible impact of radar

underestimation mentioned above. It is worth noting that this selection is only based on intensity and no other condition on rainfall amounts or rainfall preceding the high-intensity is used.

In total, we identify 11 potential initiating triggering storms that satisfy the above intensity conditions over the DFs during the periods of interest (Table 1). Nevertheless, only seven of these eleven 11 storms satisfied the conditions over all the mapped
255 DFs of a group of interest (marked by red bold text in Table 1 and blue rectangles in Fig. 56). Therefore, only seven storms can be considered as potential initiatingtriggering storms. Note, that one of them (Oct 26-29, 2015) is a potential initiating triggering storm for the DFs of two groups. We should remember that the process of identifying the triggering cell could be subject to errors so that a different storm or cell, or more than a single convective cell may have triggered the mapped DFs in a group. The procedure we adopt, however, closely follows our knowledge of DF triggering in general and of local climatology
260 of storms in particular, so this possibility is expected to be unlikely.
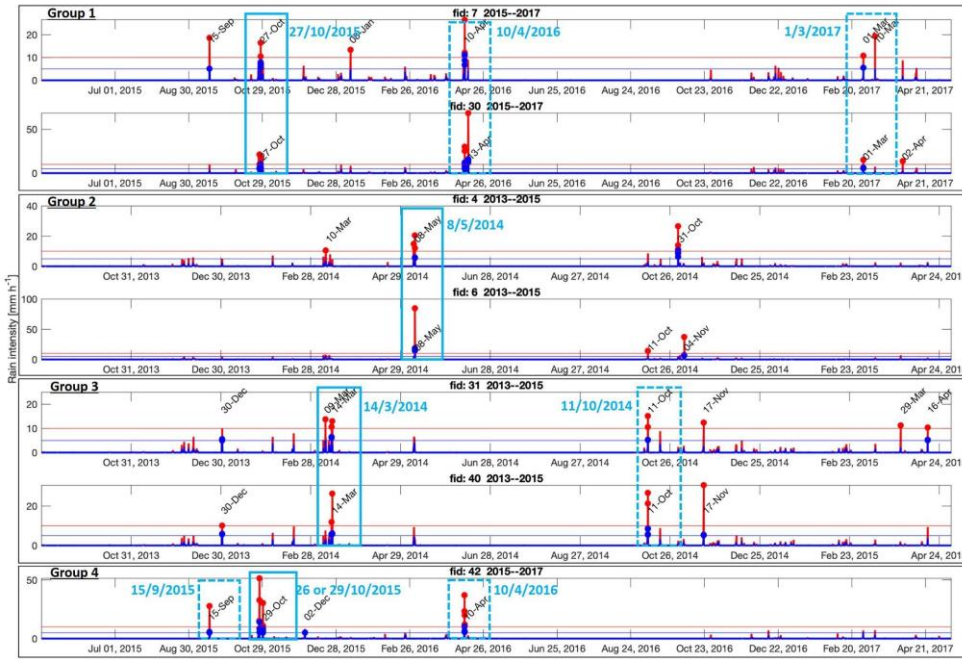
Figure 56: Time series of rainfall events over the four groups of DFs. Seven sub-plots of the rainfall intensity versus time (for two-year interval) for seven ~~different~~ DFs related to four different groups. In each sub-plot two graphs are shown: the rain intensity in 5 min interval (in red) and the smoothed intensity observed over ~~a~~ 30 min moving windows (in blue). Horizontal lines mark the two thresholds of 10 mm h⁻¹ (red) and 5 mm h⁻¹ (blue). Any storm during which the 5-min intensity exceeds~~overcomes~~ the 10 mm h⁻¹~~former~~ thresholds or the 30-min overcomes the 5 mm h⁻¹~~latter~~ threshold, is marked by a red or blue ~~coloured~~ dot, respectively. Storms exceeding both thresholds for all the DFs of a group are considered as potential ~~initiating~~ triggering storms, ~~are~~ (marked by dashed light blue box), among them, the chosen storms are marked by solid light blue box ~~lines and are highlighted in Table 1~~.

Table 1. Potential ~~initiating~~ triggering storms and suspected triggering convective cells for the 43 DFs ~~(numbered by Fid which is the object ID of a shapefile in ArcGIS Desktop)~~, organized into four groups. The DFs are numbered by Fid which is the object ID of a shapefile in ArcGIS Desktop, and in parenthesis the total number of DFs in a group is given. The weather system that produced the storms is also reported. ~~Red~~ Bold fonts indicate the potential ~~initiating~~ triggering storms.

Group number	Fid (~~DF~~ total number of DFs)	Location	Triggered between the years	Potentially ~~initiating~~ triggering storms	Suspected ~~initiating~~ triggering storm and the triggering cell	Weather system of the ~~initiating~~ triggering storm
1	7-30 (24)	Qumran - Ein-Feshkha	2015-2017	15-16/9/2015 **25-28/10/2015** **9-13/4/2016** **27/2-1/3 /2017**	25-28/10/2015 27/10/2015, 13:55-14:40	Active Red Sea Trough[a]
2	0-6 (7)	Ovnat area	2013-2015	**7-8/5/2014** 30/10-5/11 /2014	7-8/5/2014 8/5/2014, 13:50-14:10	Tropical Plume[b]
3	31-40 (10)	Metsoke Dragot	2013-2015	29-30/12/2013 **9-19/3/2014** **8-11/10/2014** 16-17/11/2014 16/4/2015	9-19/3/2014 14/3/2014, 10:35-10:55	Mediterranean Cyclone (with anomalous southern track)
4	41-42 (2)	Yishay valley	2015-2017	**14-16/9/2015** **25-29/10/2015** **9-13/4/2016**	25-29/10/2015 26/10/2015, 15:35-15:55	Active Red Sea Trough[a]

275 [a] See also Marra and Morin (2018).
 [b] See also Armon et al. (2018).

Once we identified the potential ~~initiating~~ triggering storms, we need to narrow down our choice to the most probable storm that triggered each DF group. To achieve that, we used additional analysis of the radar data, orthophotos, and online reports

280 from social media and news websites. For each of the seven potential ~~initiating~~ triggering storms we examined the event time series in terms of total rainfall and rainfall intensity versus time, for a period of hours to a few days (Fig. ~~6~~7). We also produced the 5-minute resolution rain intensity maps such as the one shown in Fig. ~~7~~8. Using those, we followed the candidate convective cells of each storm in time, and examined their spatiotemporal behavior with respect to (i) the mapped deposits and (ii) areas with similar slopes/sediment availability but no observed DF. This allowed us to narrow our choice. In some cases, such as

285 group 1 in the northern part of the study area, we could not clearly pinpoint a single triggering cell for the DFs in the group,

and we needed additional information. Using two orthophotos from the years 2015-2016 we limit our search for two out of three storms: Oct 26-27, 2015 and Apr 10-13, 2016 (Table 1). We manually searched several websites (including Facebook, Youtube and newspapers) for relevant photos and videos of floods that could help us determine the flow characteristics (debris flow or flash flood) and identify the exact timing of the event. We could only find ~~Using~~ a Facebook video showing deposits

290 on the main road (route #90) (https://www.facebook.com/chen.sason.75/videos/1155321937831332, last accessed: Apr 25, 2022), where the road crosses the most southern stream of mapped deposits from group 1 on Oct 27, 2015.~~,~~ ~~w~~We could use this information to pinpoint a specific event and a most likely triggering cell for group 1 DFs: Oct 27, 2015 between 13:55-14:40. Combining the above information, we ended up identifying the four triggering cells that, based on the information at our hand, most likely triggered the DFs in the four groups (Table 1~~, right column~~).

295
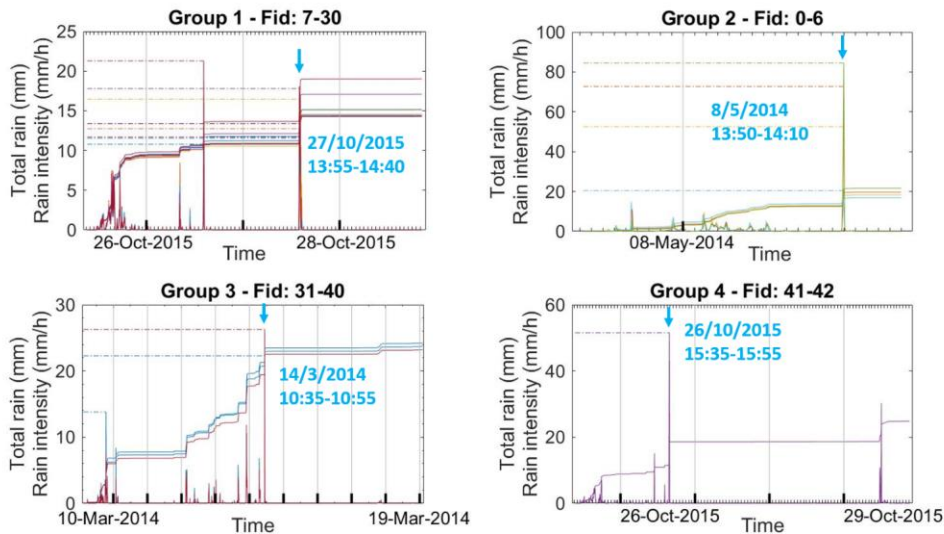
Figure ~~6~~7: Rainfall evolution over the DF locations during the ~~initiating~~ triggering storms (see Table 1). For each group we plot the intensity (spikes) and cumulative rain (stairs graph) during the ~~initiating~~ triggering storm, for all DF (where 'Fid' is the identification number of the DF) locations in the group (the different line colors). Dashed lines mark the peaks of rain intensity. A blue arrow marks the triggering

300 cell during each storm. Note, that the y-axis shows both rain intensity in mm h^{-1} and total cumulative rain during the storm in mm.

4.3 Characterization of the rainfall leading to debris flows

The characteristics of the rainfall during the ~~initiating~~ triggering storms were examined to evaluate the critical conditions for DF triggering in the study area. The triggering cells are intense and short, intensities are in the range of 10-85 mm h^{-1}, and

durations between ~about 20 min (groups 2-4) and ~45 min (group 1, Table 1 and Fig. 67). Interestingly, for all DFs, significant
antecedent ~~precipitation~~ rainfall was observed for the ~~initiating~~ triggering storms during the hours preceding the triggering cell
(usually more than 10 mm, Fig. 67). To further explore this point, we plotted for each group the spatial distribution of
antecedent ~~precipitation~~ rainfall over the study area and compared it with the spatial distribution of the total rainfall yield of
the triggering cells, and with their maximum intensities over 5- and 30-min intervals (an example of such a plot is given in
Fig. 89). Figures 8b 9b through 8d 9d present the triggering cell characteristics of group 3 (in the center of the map), and
suggest that two additional convective cells (warmer colors) north and south to the main cell passed through the studied area
at the same time. While the maximum intensities of all three cells exceeds 10 mm h^{-1}, only the central one triggered the DFs
(of group 3). Although the southern cell well covers the steep slopes (meet the steep slope and sediment conditions) and is
similar in rainfall intensity, no DF was triggered. We suggest that this is related to lower amounts of antecedent
~~precipitation~~rainfall. Differently, for the northern cell it seems that the antecedent ~~precipitation~~ rainfall condition is available,
but the cell only marginally crossed the steep slopes (the cell at its peak intensity did not cross the cliff area).
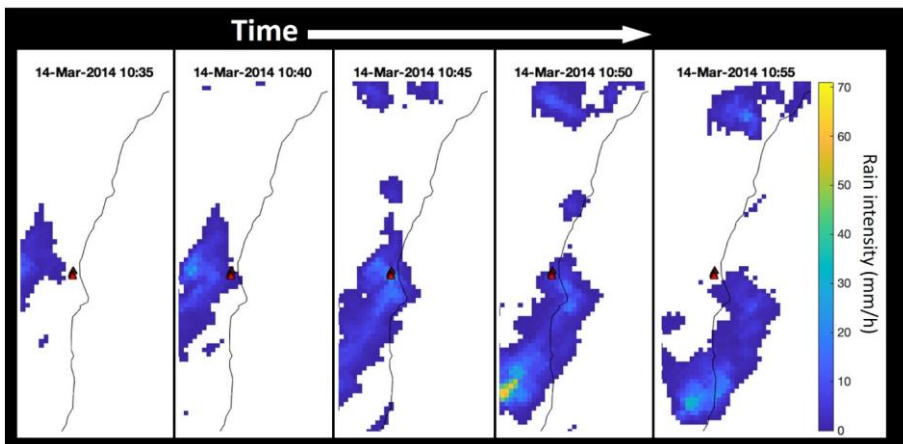
Figure 78: Weather radar maps. Time snapshots (time increases rightward) of the rain intensity over the study area during the time of the triggering cell that triggered group 3 DFs (red triangles). A black line marks the Dead-Sea shoreline. The highest rain intensities overlap the group DFs at 10:45 while the whole event is shorter than 30 min.

320
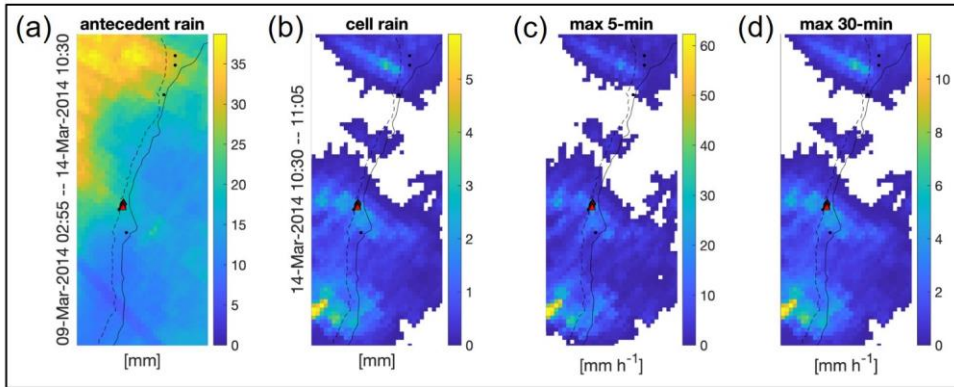
Figure 89: Rainfall leading to DFs for the event shown in Fig. 78. The cliff-top (dashed line) together with the Dead Sea shoreline (solid line), mark the narrow band of steep escarpment where debris flows may potentially be triggered. Black dots show the location of the rain gauges. (a) Antecedent ~~precipitation~~ rainfall – map of the total rainfall during the March 2014 event until the onset of the triging cell. (b) The total ~~precipitation~~ rainfall observed during the triggering cell (10:30-11:05). (c) Peak intensity of the triggering cell (5 min time interval).
325 (d) Peak intensity of the triggering cell (30 min time interval).

In order to validate the hypothesis that antecedent rainfall is an important factor in DF triggering in the study area, we examined the whole period between 2013 and 2019 with the aim of identifying storms which could potentially trigger DFs in terms of rain intensity, but did not. We focused on the triggering locations of our DFs, in order to ensure the susceptibility conditions are met. In Fig. ~~9~~ 10 we plot the antecedent rainfall versus the 5-minute rain intensity for a representative DF deposit from
330 each group. Here, the antecedent rainfall is calculated automatically over the entire time series as all the rain accumulated on the deposit pixel over the 120 hours preceding the specific measured intensity. This automatic definition provides estimates of the antecedent rainfall that are equivalent to the ones used earlier, except for the rare storms lasting longer than 5 days prior to the peak intensity; in these cases, this automatic definition might be underestimated. ~~Here, the antecedent rainfall is calculated as all the rain accumulated on the deposit pixel during the period starting on a 120 h break in rain and until the specific~~
335 ~~measured intensity.~~ For most cases, in these new graphs we picked the same potential triggering events as we previously showed (Table 1). Interestingly, for extreme intensity rainfall events ~~(>~~(exceeding 60 mm h⁻¹), like Sep 15, 2015 event in group 2 (Fig. ~~9b~~10b) and events on Jun 4, 2018 and Oct 29, 2015 in group 3 (Fig. ~~9c~~10c), no DF deposits were observed, even after re-checking the target area in our DoD.
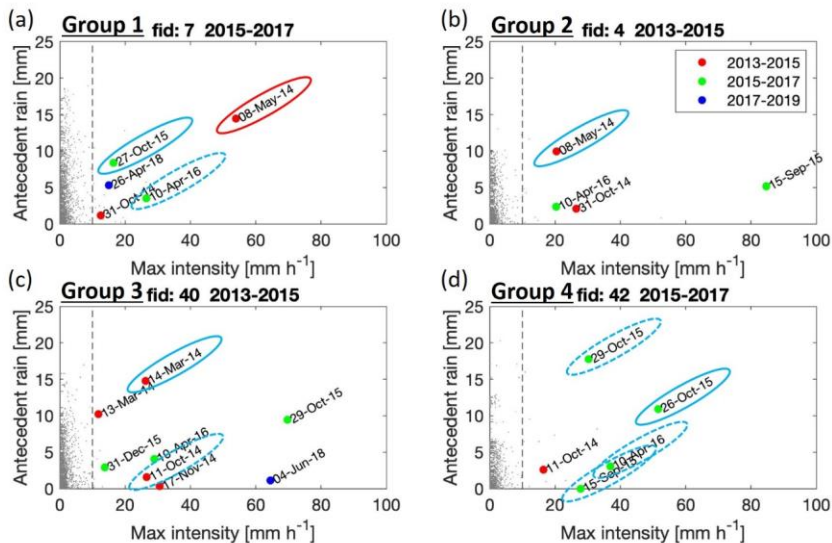
Figure 910: Scatter plots of antecedent rainfall versus maximum 5-minute rain intensity observed over four DFs representative of the four groups (a-d) for all the storms observed in the radar archive in the period 2013-2019. Data points exceeding the intensity of 10 mm h^{-1} for 5-minute intensity and 5 mm h^{-1} for 30-minute intensity are marked by color and classified according to the time interval specified by the DoDs. Potentially triggering storms (~~red~~ bolded text in Table 1) are marked with dashed blue ellipses, whereas the most likely triggering storm~~s~~ identified in this study ~~are~~is marked with a continuous blue ellipse. The red ellipse in group 1 marks the storm of May 8 2014, discussed at the end of this Section.

An interesting additional story is told by Fig. ~~9a~~10a: the event on May 8, 2014 shows relatively high antecedent ~~precipitation~~ rainfall (~~>~~more than 10 mm) as well as peak intensity (~~>~~more than 50 mm h^{-1}), compared to the likely triggering event on Oct 27, 2015, but occurred before the DFs in group 1 were triggered (they were not observed in the LiDAR flight between these two storms). Given the strong characteristics of this cell in terms of both antecedent ~~precipitation~~ rainfall and peak intensity, and since the mapping could not be fully effective for small DFs, we further examined the region around group 1 looking for potential signatures of the May 8, 2014 storm. Indeed, some tiny shallow deposits appeared during the period 2013-2015. They are located on the western edge of group 1 area, in close proximity to the May 8, 2014 cell peak. While these mass movements are small with respect to the DFs examined so far in this paper, they show similar DF-like properties. The fact that we could find new mass movements based on the requirement of both antecedent ~~precipitation~~ rainfall and peak intensity constitutes an additional element supporting our hypothesis.

5 Discussion

5.1 Characterization of the rainfall leading to debris flows in arid regions

As mentioned in section 4.3, the investigated triggering cells are intense (10-85 mm h^{-1}) and short (20-45 min) (Table 1 and
360   Fig. ~~6~~7). Both their intensities and durations are lower than the previously suggested threshold for DF triggering in the study
area (intensities ~~>~~greater than 30 mm h^{-1} for duration of one hour or longer, Ben David-Novak et al., 2004). A previous study
conducted in the arid slopes of the Grand Canyon, Arizona, cautiously suggested that sustained intensity exceeding 20 mm h^{-1}
and a total rainfall of 25 to 50 mm may be a minimum requirement for DF triggering, without mentioning a minimum duration
(Melis et al., 1995). In our study, only two out of the four triggering cells, have maximum intensities exceeding 30 mm h^{-1}, but
365   these intensities were observed only for a short period (less than~~<~~ 10 min), much shorter than what previously reported (Fig.
~~6~~7). While for most of our mapped DFs, intensity was indeed ~~>~~greater than 20 mm h^{-1} the total rainfall for all triggering cells
was ~~<~~lower than 25 mm (Fig. ~~4~~7). Quantitative accuracy of radar data, however, is not perfect and, as mentioned above,
possible underestimation cannot be excluded. Considering the limited datasets available for arid regions, it is still impossible
to determine a unique threshold for DF triggering. More attempts should focus on data collection in these regions and on
370   carefully considering the spatiotemporal distribution of rainfall during the ~~initiating~~ triggering storms. Hints towards the
importance of the temporal rain distribution during a storm could already be found in Ben David-Novak et al. (2004) as their
data showed that for both studied events the triggering cells reached the area only hours after a significant antecedent
~~precipitation~~rainfall.

We speculate that antecedent ~~precipitation~~ rainfall or the flow of water in the steep channels caused by antecedent ~~precipitation~~
375   rainfall could reduce the sediment strength by wetting. The effects of pore pressure increase and the reduction of apparent
cohesive strength most likely cause this strength reduction (Takahashi, 2014; Terzaghi, 1943). ~~The reduction of sediment~~
~~strength~~The strength reduction may be followed by enhanced incision or direct failure of the sediments within the channel.
Such slope instability can initiate the DFs once the high intensities provided by a triggering cell provide a significant water
flow at these channels. Shmilovitz et al. (2020) showed that the threshold for runoff flow on nearby desert slopes is ~14-22
380   mm h^{-1} for a duration of five minutes. This threshold is met by all the four triggering cells that we consider the most likely
trigger for the mapped DF deposits, but it is also met by many other storms among the ones we identify as possible candidates
(Table 1). We hypothesize, that due to the lack of antecedent ~~precipitation~~rainfall, no DFs were triggered by these cells. At the
same time, however, flash floods could indeed have been generated, as frequently observed along the cliff during heavy storms
(Belachsen et al., 2017).

385   **5.2 Implications for debris flow occurrence in the region**

The need for antecedent ~~precipitation~~ rainfall could also help explaining the low incidence of DFs in the area: to date, only
seven modern DF-triggering storms are reported in the study area. Four events reported for ten years period between October

1987 to October 1997 (Ben David-Novak, 1998; Ben David-Novak et al., 2004) and three identified in the current study – roughly equivalent to one ~~initiating~~ triggering storm every two-three years. Given the vast sediment availability, the rarity of DFs in the area is usually explained by the dry weather (i.e., low number of storms) and the small areal extent of the susceptible steep slopes: only convective cells hitting the small susceptible area can trigger a DF. However, while storms in the area are indeed not frequent, each storm usually brings numerous convective cells. Belachsen et al. (2017) identified 424 storms in the area in the period 1990-2014, about ~20 per year, associated with over 10,000 convective cells, an average of ~~>~~over 24 cells per storm. Similarly, Marra and Morin (2018) showed that individual storms can bring even hundreds of high-intensity convective cells. With these numbers, it is more difficult to motivate the rarity of DFs just using the reasoning above. Conversely, the here suggested need for antecedent ~~precipitation~~ rainfall as a prerequisite for the triggering implies a need for an intense convective cell to hit an area where non-negligible precipitation already occurred during the same storm.

The need for antecedent ~~precipitation~~ rainfall as a critical triggering condition also in arid areas could facilitate the prediction of such events. Heavy rain intensity remains a key trigger of DFs, but the trajectory and intensity of convective cells cannot be forecasted with sufficient accuracy even with the most advanced weather models (e.g., see Rinat et al., 2021). In addition, the short distance between the debris sources and the vulnerable structures drastically reduces the effectiveness of warnings based on radar nowcasting (e.g., Sideris et al., 2020). Conversely, antecedent ~~precipitation~~ rainfall can be monitored more easily during the storm, for example using weather radar observations, and then used to highlight areas more susceptible to possible incoming convective cells. This information could be used to send targeted warnings to the relevant locations and structures at risk.

5.3 Limitations of this study

Our results are based on a relatively small sample of small-sized DFs detected in an arid region of the eastern Mediterranean. Although we extensively explored the region in Figure 1, this inventory cannot be considered complete because DFs could have been missed due to noise in the LiDAR data or other data issues (e.g. see Section 4.3). In addition, weather radar uncertainties may affect the precipitation estimates (e.g., see Marra et al., 2022). One source of uncertainty in particular is worth mentioning: the possible advection of precipitation during its falling from the height of the radar sampling volume ~~(~~(about 3 km above the ground level) and the ground could lead to misplacements of the radar estimates of few hundreds of meters; this would typically lead to an underestimation of the rainfall amounts (Marra et al., 2016). In addition, it is important to recall that the adjustment of the radar data is based on few available stations: some level of uncertainty in the quantitative estimates is thus to be expected. While our qualitative results are robust with respect to these sources of error and support our reasoning in terms of process description and understanding, the numbers are subject to residual uncertainty and caution is advised against their direct use in warning systems.

6 Conclusions

In this paper, we investigate the rainfall conditions leading to DFs in steep arid slopes, where the lack of DF observations and
420   rainfall data still hinders our understanding of the typical triggering conditions. We use high-resolution topography, and field
surveys ~~and social media information~~ to map over 40 deposits resulted from DFs in the arid region of the Dead Sea western
escarpment during 2013-2019. We then use high-resolution weather radar rainfall to pick the most likely ~~initiating~~ triggering
storms and estimates to investigate the rainfall conditions leading to the ~~initiation~~ triggering of DFs in terms of peak intensity
and rainfall amounts prior to the triggering convective cell.

425   The spatial and temporal analysis of the mapped deposits and of weather radar data over the triggering locations, suggests that
the 43 identified DFs were triggered by three storms occurred during the spring of 2014 and the autumn of 2015. The mapped
deposits were likely triggered by short convective cells which usually lasted less than 30 minutes and could show peak
intensities lower than 30 mm h^{-1}. These numbers are lower compared to previous studies based on two events in the area (>30
mm h^{-1} for ~~>~~over 1 hour). Comparing triggering and non-triggering storms, we suggest that antecedent ~~precipitation~~ rainfall
430   during the hours to days prior to the triggering convective cells may play a critical role for DF triggering in arid steep slopes.
We speculate that wetting of the slope sediments could reduce it strength and allow its massive drift during the channel flow
caused by the main convective cell. Our hypothesis is supported by the observation of numerous convective cells with
intensities similar or greater than the triggering ones but no DF signature appears in the topography even in susceptible
locations, such as the location of DFs triggered by subsequent storms. In addition, our hypothesis could help explaining the
435   very low occurrence frequency of DFs in an area with high susceptibility and relatively frequent high-intensity convective
cells. Our findings bring new information to our understanding of DF triggering in arid regions and could be included in
regional-scale warning systems to help minimizing the hazard potential of these events.

Data availability

Rain gauge data were provided and pre-processed by the Israel Meteorological Service and are freely available at https://ims.data.gov.il/ (last access: 13 March 2022, Hebrew only). Corrected weather radar data were made available by the Hydrometeorology lab at the Hebrew University of Jerusalem and cannot be directly shared by the authors; the data can be requested to the Hydrometeorology lab at https://hydrometeorology-lab.huji.ac.il/book/contact-us (last accessed 28 June 2022). Orthophotos are the product of the Survey of Israel, and are available according to their policy. For further information, please contact the Survey by email: tatsa@mapi.gov.il. Airborne LiDAR scans ordered by the Geological Survey of Israel from Ofek Aerial Photography. The original scans cannot be shared online. Please contact the corresponding author for further information.

Author contribution

SST conducted mapping and fieldwork, data curation and formal analysis, funding acquisition, and wrote the original draft. FM was responsible for rainfall data curation and formal analysis. Both authors conceptualized the study and contributed to the writing – review & editing.

Competing interests

The authors declare that they have no conflict of interest.

Acknowledgments

We thank Efrat Morin, Yehuda Enzel and Oded Katz for fruitful discussions and Moshe Armon for the synoptic classification of the storms. We also thank Yair Rinat, Hallel Lutsky, and Jonathan Levy for their assistance in the field work. This work was funded by the Geological Survey of Israel, Dead-Sea project #40832. FM was supported by internal funds of the Institute of Atmospheric Sciences and Climate of the National Research Council of Italy (CNR-ISAC) and by the CARIPARO Foundation through the Excellence Grant 2021 to the "Resilience" Project.

References

Ahlborn, M., Armon, M., Ben Dor, Y., Neugebauer, I., Schwab, M. J., Tjallingii, R., Shoqeir, J. H., Morin, E., Enzel, Y., and Brauer, A.: Increased frequency of torrential rainstorms during a regional late Holocene eastern Mediterranean drought, Quat. Res. (United States), 89, 425–431, https://doi.org/10.1017/qua.2018.9, 2018.

Aleotti, P.: A warning system for rainfall-induced shallow failures, Eng. Geol., 73, 247–265, https://doi.org/10.1016/j.enggeo.2004.01.007, 2004.

Armon, M., Dente, E., Smith, J. A., Enzel, Y., and Morin, E.: Synoptic-scale control over modern rainfall and flood patterns in the Levant drylands with implications for past climates, J. Hydrometeorol., 19, 1077–1096, https://doi.org/10.1175/JHM-D-18-0013.1, 2018.

Armon, M., Morin, E., and Enzel, Y.: Overview of modern atmospheric patterns controlling rainfall and floods into the Dead Sea: Implications for the lake's sedimentology and paleohydrology, Quat. Sci. Rev., 216, 58–73, https://doi.org/https://doi.org/10.1016/j.quascirev.2019.06.005, 2019.

Bartov, Y., Stein, M., Enzel, Y., Agnon, A., and Reches, Z.: Lake levels and sequence stratigraphy of Lake Lisan, the late Pleistocene precursor of the Dead Sea, Quat. Res., 57, 9–21, https://doi.org/10.1006/qres.2001.2284, 2002.

Bartov, Y., Enzel, Y., Porat, N., and Stein, M.: Evolution of the Late Pleistocene-Holocene Dead Sea basin from sequence statigraphy of fan deltas and lake-level reconstruction, J. Sediment. Res., 77, 680–692, https://doi.org/10.2110/jsr.2007.070, 2007.

Begin, Z. B., Nathan, Y., and Ehrlich, A.: Stratigraphy and facies distribution in the Lisan Formation—new evidence from the area south of the Dead Sea, Israel, Isr. J. Earth Sci., 29, 182–189, 1980.

Belachsen, I., Marra, F., Peleg, N., and Morin, E.: Convective rainfall in a dry climate: Relations with synoptic systems and flash-flood generation in the Dead Sea region, Hydrol. Earth Syst. Sci., 21, 5165–5180, https://doi.org/10.5194/hess-21-5165-2017, 2017.

Blackwelder, E.: Mudflow as a geologic agent in semiarid mountains, Bull. Geol. Soc. Am., 39, 465–484, https://doi.org/10.1130/GSAB-39-465, 1928.

Brand, E. W.: Slope instability in tropical areas., in: Proceedings of the 6th International Symposium on Landslides, 2031–2051, 1992.

Caine, N.: The rainfall intensity-duration control of shallow landslides and debris flows., Geogr. Ann. Ser. A, 62, 23–27, https://doi.org/10.1080/04353676.1980.11879996, 1980.

Church, M. and Miles, M. J.: Meteorological antecedents to debris flow in southwestern British Columbia; some case studies, Rev. Eng. Geol., IVV, 63–80, 1987.

Coe, J. A., Glancy, P. A., and Whitney, J. W.: Volumetric analysis and hydrologic characterization of a modern debris flow near Yucca Mountain, Nevada, 20, 11–28, https://doi.org/10.1016/s0169-555x(97)00008-1, 1997.

Corominas, J. and Moya, J.: Reconstructing recent landslide activity in relation to rainfall in the Llobregat River basin, Eastern Pyrenees, Spain, 30, 79–93, https://doi.org/10.1016/S0169-555X(99)00046-X, 1999.

Costa, J. E.: Rheologic, geomorphic, and sedimentologic differentiation of water floods, hyperconcentrated flows, and debris

flows, Flood Geomorphol., 113–122, 1988.

495 Ben David-Novak, H.: Modern and Holocene debris flows along the western escarpment of the Dead-Sea (in Hebrew), The Hebrew University of Jerusalem, 129 pp., 1998.

Ben David-Novak, H., Morin, E., and Enzel, Y.: Modern extreme storms and the rainfall thresholds for initiating debris flow on the hyperarid western escarpment of the Dead Sea, Israel, Bull. Geol. Soc. Am., 116, 718–728, https://doi.org/10.1130/B25403.2, 2004.

500 Destro, E., Marra, F., Nikolopoulos, E. I., Zoccatelli, D., Creutin, J. D., and Borga, M.: Spatial estimation of debris flows-triggering rainfall and its dependence on rainfall return period, 278, 269–279, https://doi.org/10.1016/j.geomorph.2016.11.019, 2017.

Dunkerley, D.: Rainfall intensity in geomorphology: Challenges and opportunities, Prog. Phys. Geogr., 45, 488–513, https://doi.org/10.1177/0309133320967893, 2021.

505 Enzel, Y.: Holocene debris flows along the western escarpment of the Dead Sea basin: Israel Ministry of Infrastructure, Earth Sciences Administration Report ES-53-2001 (in Hebrew), 28 pp., 2001.

Frattini, P., Crosta, G., and Sosio, R.: Approaches for defining thresholds and return periods for rainfall-triggered shallow landslides, Hydrol. Process., 23, 1444–1460, https://doi.org/10.1002/hyp.7269, 2009.

Garfunkel, Z. and Ben-Avraham, Z.: The structure of the Dead Sea basin, 266, 155–176, 1996.

510 Garfunkel, Z., Zak, I., and Freund, R.: Active faulting in the dead sea rift, 80, 1–26, 1981.

Glade, T., Crozier, M., and Smith, P.: Applying probability determination to refine landslide-triggering rainfall thresholds using an empirical "Antecedent Daily Rainfall Model," Pure Appl. Geophys., 157, 1059–1079, https://doi.org/10.1007/s000240050017, 2000.

Griffiths, P. G.: Frequency and initiation of debris flows in Grand Canyon, Arizona, J. Geophys. Res., 109, 515 https://doi.org/10.1029/2003jf000077, 2004.

Guzzetti, F., Peruccacci, S., Rossi, M., and Stark, C. P.: The rainfall intensity-duration control of shallow landslides and debris flows: An update, 5, 3–17, https://doi.org/10.1007/s10346-007-0112-1, 2008.

Haviv, I., Enzel, Y., Whipple, K. X., Zilberman, E., Stone, J., Matmon, A., and Fifield, L. K.: Amplified erosion above waterfalls and oversteepened bedrock reaches, J. Geophys. Res. Earth Surf., 111, https://doi.org/10.1029/2006JF000461, 2006.

520 Hochman, A., Marra, F., Messori, G., Pinto, J. G., Raveh-Rubin, S., Yosef, Y., and Zittis, G.: Extreme weather and societal impacts in the eastern Mediterranean, Earth Syst. Dyn., 13, 749–777, https://doi.org/10.5194/esd-13-749-2022, 2022.

Hungr, O., Evans, S. G., Bovis, M. J., and Hutchinson, J. N.: A review of the classification of landslides of the flow type, Environ. Eng. Geosci., https://doi.org/10.2113/gseegeosci.7.3.221, 2001.

Iverson, R. M.: The physics of debris flows, Rev. Geophys., 35, 245–296, https://doi.org/10.1029/97RG00426, 1997.

525 Iverson, R. M.: Landslide triggering by rain infiltration, Water Resour. Res., 36, 1897–1910, https://doi.org/10.1029/2000WR900090, 2000.

Kim, S. W., Chun, K. W., Kim, M., Catani, F., Choi, B., and Seo, J. Il: Effect of antecedent rainfall conditions and their variations on shallow landslide-triggering rainfall thresholds in South Korea, 18, 569–582, https://doi.org/10.1007/s10346-020-01505-4, 2021.

530 Marra, F. and Morin, E.: Use of radar QPE for the derivation of Intensity-Duration-Frequency curves in a range of climatic regimes, J. Hydrol., 531, 427–440, https://doi.org/10.1016/j.jhydrol.2015.08.064, 2015.

Marra, F. and Morin, E.: Autocorrelation structure of convective rainfall in semiarid-arid climate derived from high-resolution X-Band radar estimates, Atmos. Res., 200, 126–138, https://doi.org/10.1016/j.atmosres.2017.09.020, 2018.

Marra, F., Nikolopoulos, E. I., Creutin, J. D., and Borga, M.: Radar rainfall estimation for the identification of debris-flow occurrence thresholds, J. Hydrol., 519, 1607–1619, https://doi.org/10.1016/j.jhydrol.2014.09.039, 2014.

Marra, F., Nikolopoulos, E. I., Creutin, J. D., and Borga, M.: Space–time organization of debris flows-triggering rainfall and its effect on the identification of the rainfall threshold relationship, J. Hydrol., 541, 246–255, https://doi.org/10.1016/j.jhydrol.2015.10.010, 2016.

Marra, F., Armon, M., and Morin, E.: Coastal and orographic effects on extreme precipitation revealed by weather radar observations, Hydrol. Earth Syst. Sci., 26, 1439–1458, https://doi.org/10.5194/hess-26-1439-2022, 2022.

Melis, T. S. and Webb, R. H.: Debris flows in Grand Canyon National Park, Arizona: magnitude, frequency and effects on the Colorado River, in: Proceedings - National Conference on Hydraulic Engineering, 1290–1295, 1993.

Melis, T. S., Webb, R. H., Griffiths, P. G., and Wise, T. W.: Magnitude and frequency data for historic debris flows in Grand Canyon National Park and vicinity, Arizona, U. S. Geological Water-Resources Investigations Report 94-4214, 285 pp., 1995.

545 Mor, U.: The geology of the Judean Desert in the area of Nahal Darga (in Hebrew), GSI/21/87, Jerusalem, 112 pp., 1987.

Moreiras, S. M. and Sepúlveda, S. A.: Landslides in Arid and Semi-Arid Environments, in: Treatise on Geomorphology, Elsevier, 322–337, https://doi.org/10.1016/b978-0-12-818234-5.00105-x, 2022.

Morino, C., Conway, S. J., Balme, M. R., Hillier, J., Jordan, C., Sæmundsson, Þ., and Argles, T.: Debris-flow release processes investigated through the analysis of multi-temporal LiDAR datasets in north-western Iceland, Earth Surf. Process. Landforms,
550 44, 144–159, https://doi.org/10.1002/esp.4488, 2019.

Mostbauer, K., Kaitna, R., Prenner, D., and Hrachowitz, M.: The temporally varying roles of rainfall, snowmelt and soil moisture for debris flow initiation in a snow-dominated system, Hydrol. Earth Syst. Sci., 22, 3493–3513, https://doi.org/10.5194/hess-22-3493-2018, 2018.

Nikolopoulos, E. I., Crema, S., Marchi, L., Marra, F., Guzzetti, F., and Borga, M.: Impact of uncertainty in rainfall estimation
555 on the identification of rainfall thresholds for debris flow occurrence, 221, 286–297, https://doi.org/10.1016/j.geomorph.2014.06.015, 2014.

Nikolopoulos, E. I., Borga, M., Creutin, J. D., and Marra, F.: Estimation of debris flow triggering rainfall: Influence of rain gauge density and interpolation methods, 243, 40–50, https://doi.org/10.1016/j.geomorph.2015.04.028, 2015.

Peleg, N. and Morin, E.: Convective rain cells: Radar-derived spatiotemporal characteristics and synoptic patterns over the
560 eastern Mediterranean, J. Geophys. Res., 117, D15116, https://doi.org/10.1029/2011JD017353, 2012.

Pierson, T.: Distinguishing between debris flows and floods from field evidence in small watersheds, 4, 2005.

Rahardjo, H., Li, X. W., Toll, D. G., and Leong, E. C.: The effect of antecedent rainfall on slope stability, Geotech. Geol. Eng., 19, 371–399, https://doi.org/10.1023/A:1013129725263, 2001.

Raz, E.: The geology of the Judean Desert, Ein Gedi area (in Hebrew), GSI\S3\1983, Jerusalem, 110 pp., 1983.

565 Rinat, Y., Marra, F., Armon, M., Metzger, A., Levi, Y., Khain, P., Vadislavsky, E., Rosensaft, M., and Morin, E.: Hydrometeorological analysis and forecasting of a 3-day flash-flood-triggering desert rainstorm, Nat. Hazards Earth Syst. Sci., 21, 917–939, https://doi.org/10.5194/nhess-21-917-2021, 2021.

Roth, I.: The geology Wadi el-Qilt area (in Hebrew), M.Sc. thesis, The Hebrew University of Jerusalem, 82 pp., 1969.

Sepúlveda, S. A., Rebolledo, S., and Vargas, G.: Recent catastrophic debris flows in Chile: Geological hazard, climatic
570 relationships and human response, Quat. Int., 158, 83–95, https://doi.org/10.1016/j.quaint.2006.05.031, 2006.

Sepúlveda, S. A., Rebolledo, S., McPhee, J., Lara, M., Cartes, M., Rubio, E., Silva, D., Correia, N., and Vásquez, J. P.: Catastrophic, rainfall-induced debris flows in Andean villages of Tarapacá, Atacama Desert, northern Chile, 11, 481–491, https://doi.org/10.1007/s10346-014-0480-2, 2014.

Shmilovitz, Y., Morin, E., Rinat, Y., Haviv, I., Carmi, G., Mushkin, A., and Enzel, Y.: Linking frequency of rainstorms, runoff
575 generation and sediment transport across hyperarid talus-pediment slopes, Earth Surf. Process. Landforms, 45, 1644–1659, https://doi.org/10.1002/esp.4836, 2020.

Sideris, I. V, Foresti, L., Nerini, D., and Germann, U.: NowPrecip: localized precipitation nowcasting in the complex terrain of Switzerland, Q. J. R. Meteorol. Soc., 146, 1768–1800, https://doi.org/https://doi.org/10.1002/qj.3766, 2020.

Sneh, A.: Late Pleistocene fan-deltas along the Dead Sea Rift, Soc. Econ. Paleontol. Mineral. Spec. Publ., 49, 541–552, 1979.

580 Sneh, A., Bartov, Y., and Weissbrod, T.: Stratigraphic chart of exposed rock-units in Israel, 2000.

Stolle, A., Langer, M., Blöthe, J. H., and Korup, O.: On predicting debris flows in arid mountain belts, Glob. Planet. Change, 126, 1–13, https://doi.org/10.1016/j.gloplacha.2014.12.005, 2015.

Takahashi, T.: Debris Flow: Mechanics, Prediction and Countermeasures, 2nd edition, CRC Press, 572 pp., 2014.

Terzaghi, K.: Theoretical soil mechanics, J. Wiley and Sons, inc., New York, 510 pp., https://doi.org/10.1002/9780470172766,
585 1943.

Tubi, A. and Dayan, U.: Tropical Plumes over the Middle East: Climatology and synoptic conditions, Atmos. Res., 145–146, 168–181, https://doi.org/10.1016/j.atmosres.2014.03.028, 2014.

Webb, R. H., Pringle, P. T., and Rink, G. R.: Debris Flows from Tributaries of the Colorado River, Grand Canyon National Park, Arizona, 1989.

590 Wells, S. G. and Harvey, A. M.: Sedimentologic and geomorphic variations in storm-generated alluvial fans, Howgill Fells, northwest England., Geol. Soc. Am. Bull., 98, 182–198, https://doi.org/10.1130/0016-7606(1987)98<182:SAGVIS>2.0.CO;2, 1987.

Williams, R. D.: DEMs of Difference, Geomorphol. Tech., 2, 1–17, 2012.

Zoccatelli, D., Marra, F., Armon, M., Rinat, Y., Smith, J. A., and Morin, E.: Contrasting rainfall-runoff characteristics of floods

595   in desert and Mediterranean basins, Hydrol. Earth Syst. Sci., 23, 2665–2678, https://doi.org/10.5194/hess-23-2665-2019, 2019.